



**HAL**  
open science

## Pearlite in hypoeutectoid iron–nitrogen binary alloys

X. C. Xiong, A. Redjaïmia, M. Gouné

► **To cite this version:**

X. C. Xiong, A. Redjaïmia, M. Gouné. Pearlite in hypoeutectoid iron–nitrogen binary alloys. *Journal of Materials Science*, 2009, 44, pp.632-638. 10.1007/s10853-008-3054-7 . hal-04559990

**HAL Id: hal-04559990**

**<https://hal.univ-lorraine.fr/hal-04559990v1>**

Submitted on 26 Apr 2024

**HAL** is a multi-disciplinary open access archive for the deposit and dissemination of scientific research documents, whether they are published or not. The documents may come from teaching and research institutions in France or abroad, or from public or private research centers.

L'archive ouverte pluridisciplinaire **HAL**, est destinée au dépôt et à la diffusion de documents scientifiques de niveau recherche, publiés ou non, émanant des établissements d'enseignement et de recherche français ou étrangers, des laboratoires publics ou privés.



Distributed under a Creative Commons Attribution 4.0 International License

# Pearlite in hypoeutectoid iron–nitrogen binary alloys

X. C. Xiong · A. Redjaïmia · M. Gouné

Received: 6 March 2008 / Accepted: 15 October 2008 / Published online: 10 November 2008  
© Springer Science+Business Media, LLC 2008

**Abstract** In this study, hypoeutectoid Fe–N binary specimens have been prepared by gas nitriding pure iron in austenite domain at 840 °C. The slow cooling of these specimens led to the  $\alpha$ -ferrite +  $\gamma'$ -Fe<sub>4</sub>N pearlitic microstructure which is similar to the pearlite in Fe–C binary system. This pearlitic microstructure has been characterized by electron microscopy. The crystal structure of the  $\gamma'$ -Fe<sub>4</sub>N nitride has been identified by electron microdiffraction and the Nishiyama–Wassermann (N–W) and near Kurdjumov–Sachs (K–S) orientation relationships have been found between the  $\alpha$ -ferrite and the  $\gamma'$ -Fe<sub>4</sub>N.

## Introduction

The substitution of carbon by nitrogen as an interstitial element in metallurgy is of considerable interest, because, compared to carbon, nitrogen has some advantages: higher maximum interstitial concentration in ferrite and in austenite, leading to higher solid-solution strengthening effect in ferrite [1–5] and higher austenite stability [1–4, 6], respectively; lower eutectoid temperature leading to lower energy consumption for some heat treatments [1–4]. For these reasons, the nitrogen steels with low alloy elements content is one of the concerns in the development of high strength steels. The role of nitrogen is now well apprehended in the stainless high nitrogen steels [7]. However, it

has rarely been studied in the pearlitic, Dual-Phase and TRIP Fe–N binary steels. One of the principal reasons for this lack of interest is related to the very low nitrogen solubility in iron liquid (0.046 wt% at 1,600 °C) [7, 8], in which the alloy elements are added during steelmaking. This low solubility of nitrogen in iron liquid is a barrier to the development of high strength nitrogen steels by traditional processes.

The iron–nitrogen system, similar to the iron–carbon system, undergoes an eutectoid transformation which leads to the decomposition of austenite at the eutectoid point (592 °C and 2.4 wt%). This eutectoid product, composed of  $\alpha$ -ferrite and  $\gamma'$ -Fe<sub>4</sub>N nitride, is labelled nitrogen pearlite because of its similarity to the lamellar carbon pearlite. This lamellar pearlitic microstructure was first observed in 1905 by Braune [9]. In 1923, Fry [10] named the structure “Braunite”. To our knowledge, this nitrogen pearlite has not been studied intensively [9–13] because of little industrial interest compared with the carbon pearlite. Detailed investigations focused on the morphology and the crystallography of the nitrogen pearlite have not been reported since the initiation of the study by Bell and Farnell [13] in 1971.

In this study, nitrogen pearlite specimens have been prepared by gas nitriding in austenitic range. The crystallography of the  $\gamma'$ -Fe<sub>4</sub>N nitride has been confirmed by electron microdiffraction and its orientation relationship with the ferrite has been derived. The morphology of the lamellar and granular structure has been studied by scanning and transmission electron microscopy.

## Experimental procedure

Pure iron sheets of 0.75 mm thickness were nitrided at 840 °C in ammonia–hydrogen gas mixtures, the

X. C. Xiong · A. Redjaïmia (✉) · M. Gouné  
Laboratoire de Science et Génie des Surfaces, Nancy-Université,  
CNRS, Parc de Saurupt CS 14234, 54042 Nancy, France  
e-mail: Abdelkrim.Redjaïmia@mines.inpl-nancy.fr

M. Gouné  
ArcelorMittal SA, Voie Romaine, BP 30320,  
57283 Maizières-les-Metz, France

composition of which is  $\text{NH}_3:\text{H}_2 = 1.3\%:98.7\%$  [14]. The nitriding potential  $\frac{P_{\text{NH}_3}}{P_{\text{H}_2}^{3/2}}$ , the activity of nitrogen  $a_{\text{N}}$  and the nitrogen content  $[\%N]_0$  fixed at the specimen surface are calculated to be  $\frac{P_{\text{NH}_3}}{P_{\text{H}_2}^{3/2}} = 4.19 \times 10^{-5}$ ,  $a_{\text{N}} = 1.58$  and  $[\%N]_0 = 1.2$ , respectively. Further information about nitriding procedure will be given elsewhere [15].

After nitriding, specimens were maintained at 840 °C in  $\text{N}_2$  gas flow for 1h20 for homogenizing nitrogen distribution and were cooled slowly in furnace (cooling rate = 20 °C/min). Nitrogen content (around 0.2 wt%) was controlled and measured by thermobalance and confirmed by chemical analysis. The specimen homogeneity was checked by microhardness test and metallographic observation.

Both light and scanning electron microscopy (SEM) observations were made by etching the specimen surface in a fluohydric acid-based solution. The preparation of thin foil specimens for transmission electron microscopy (TEM) examination was achieved by using double-jet technique with a 95% glacial acetic acid–5% perchloric acid electrolyte and finished by an ionic bombardment during 1 h using small attack angles. The TEM used in this investigation is the Philip CM12 operated at 120 kV. X-ray diffraction measurements were made with nickel filtered cobalt radiation ( $\lambda_{\text{CoK}\alpha} = 0.17889 \text{ nm}$ ).

**Results**

**Microstructure after slow cooling**

The nitriding, homogenization treatment and slow cooling led to a uniform microstructure (Fig. 1a). The corresponding microhardness test confirms this homogeneous nitrogen distribution (Fig. 1b). Figure 1b shows also an increase of 70 HV points of hardness, caused by the nitrogen addition, with respect to the pure iron.

The SEM observation (Fig. 2) of this hypoeutectoid Fe–N alloy highlights the existence of islands of an eutectoid lamellar structure surrounded by proeutectoid

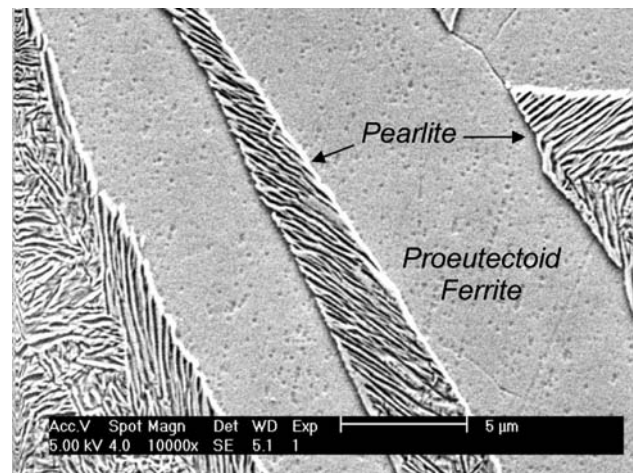


**Fig. 2** SEM micrograph of nitrogen pearlite surrounded by proeutectoid ferrite

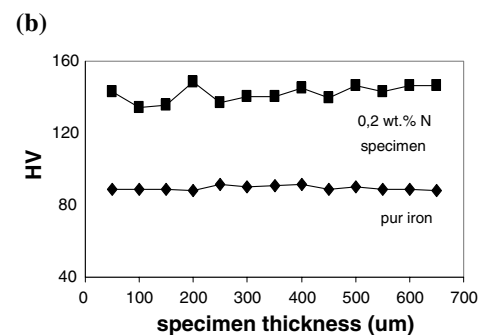
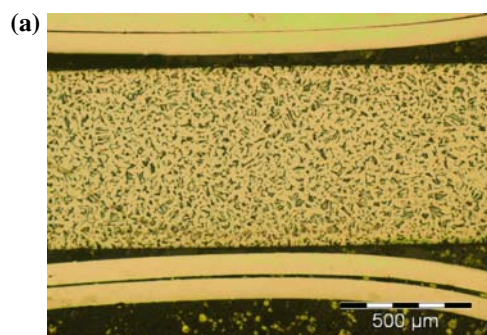
ferrite. This lamellar structure recalls the Fe–C pearlitic one. The TEM dark-field image (Fig. 3) indicates that this structure is compound of alternated lamellas of ferrite and of iron nitride, which could be  $\gamma\text{-Fe}_4\text{N}$  according to the Fe–N binary diagram. In order to identify this nitride and determine the orientation relationships between the ferrite and the nitride, a series of TEM investigations has been conducted by applying a systematic microdiffraction method [16, 17].

**Identification of the nitride  $\gamma\text{-Fe}_4\text{N}$**

The procedure of this characterization is briefly presented as follows:

- (1) The “net” symmetries for the Zero Order Laue Zones (ZOLZ) recorded along  $\langle 001 \rangle$  and  $\langle 111 \rangle$  zone axes are (4 mm) and (6 mm) (Fig. 4), respectively. These “net” symmetries correspond to a cubic system;
- (2) The shift and the periodicity difference between the ZOLZ and FOLZ (First Order Laue Zone) reflection nets along slightly tilted  $\langle 001 \rangle$  and  $\langle 011 \rangle$  zone axes [18] are related to the P– – extinction symbol

**Fig. 1 a** Light micrograph and **b** corresponding microhardness evolution of 0.2 wt% specimen nitrided and slowly cooled in furnace



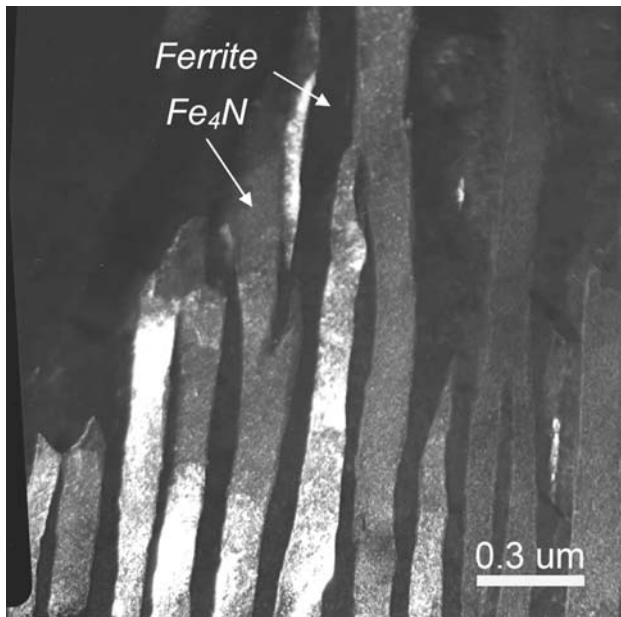


**Fig. 3** Dark-field TEM image of nitrogen pearlite

(Fig. 5), which may be associated with six spaces groups;

- (3) The “ideal” ZOLZ symmetries recorded along  $\langle 001 \rangle$ ,  $\langle 011 \rangle$  and  $\langle 111 \rangle$  zone axes (Fig. 4) are (4 mm),

**Fig. 4**  $\langle 001 \rangle$ ,  $\langle 011 \rangle$  and  $\langle 111 \rangle$  electron microdiffraction ZAPs for the  $\gamma'$ -Fe<sub>4</sub>N nitride

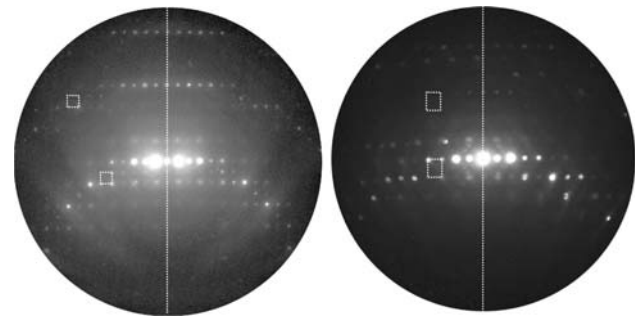
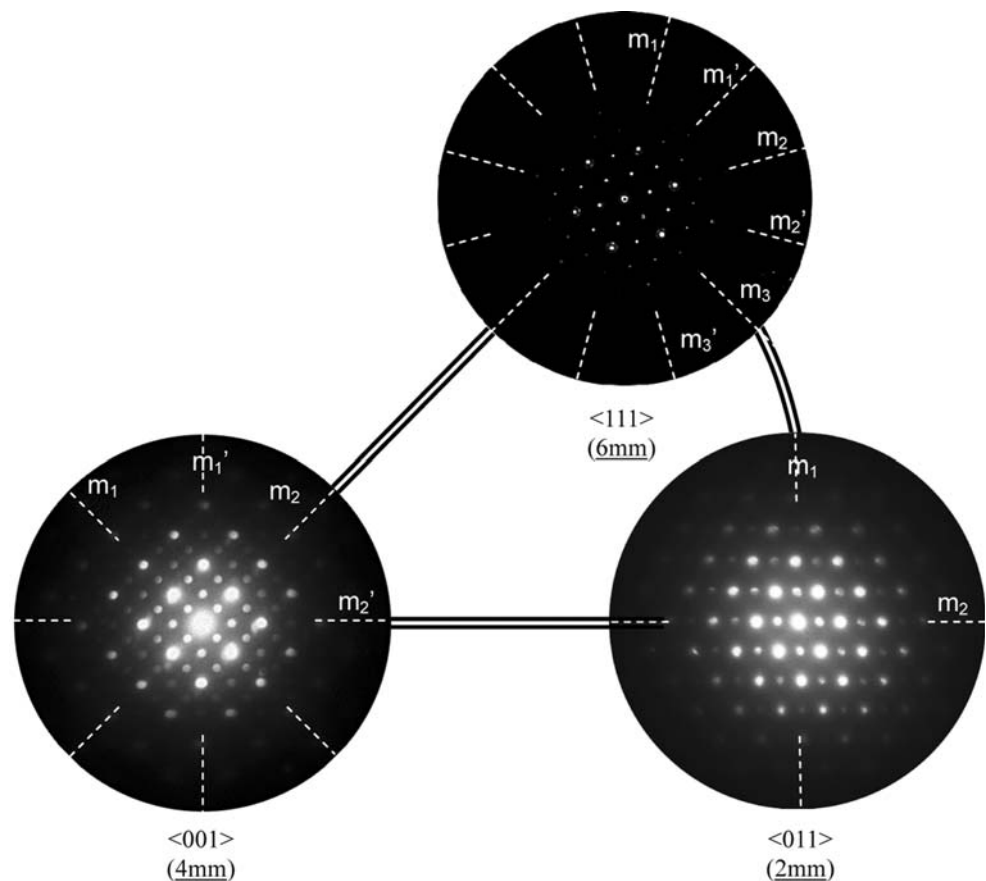


**Fig. 5** Tilted electron microdiffraction patterns along  $\langle 001 \rangle$  and  $\langle 011 \rangle$  showing ZOLZ and HOLZ areas

(2 mm) and (6 mm), respectively. These “ideal” symmetries lead to the  $m\bar{3}m$  point group.

This procedure leads to the unambiguous conclusion that the space group for the present nitride is  $Pm\bar{3}m$ , or  $P\frac{4}{m}\bar{3}\frac{2}{m}$  in its full crystallographic notation. From the  $P\frac{4}{m}\bar{3}\frac{2}{m}$  space group and the lattice parameter  $a = 0.379$  nm measured by X-ray diffraction, it is confirmed that the nitride  $\gamma'$ -Fe<sub>4</sub>N, together with the  $\alpha$ -ferrite, is effectively one of the constituents of the lamellar pearlite. As described in the literature [8], the  $\gamma'$ -Fe<sub>4</sub>N nitride lattice, belonging to the primitive cubic system, has the same iron atom arrangement as the austenite (FCC), plus a nitrogen

atom occupying the  $(\frac{1}{2}, \frac{1}{2}, \frac{1}{2})$  position in a fully ordered manner.

Ferrite–Fe<sub>4</sub>N Orientation relationships

Several electron diffraction patterns have been taken simultaneously on the ferrite and on the  $\gamma'$ -Fe<sub>4</sub>N lamellas. For most of the lamellar structure, the well-known Nishiyama–Wassermann (N–W) [19, 20] orientation relationship has been found between the  $\alpha$ -ferrite and the  $\gamma'$ -Fe<sub>4</sub>N nitride (Fig. 6). This orientation relationship can be written as follows:

$$\begin{aligned} (011)\alpha // (111)\gamma' \\ [100]\alpha // [\bar{1}\bar{1}0]\gamma' \\ [0\bar{1}1]\alpha // [\bar{1}\bar{1}2]\gamma' \end{aligned}$$

In some rare cases, a near Kurdjumov–Sachs (K–S) orientation relationship [21] has also been found (Fig. 7). The exact K–S orientation relationship is given by:

$$\begin{aligned} (011)\alpha // (111)\gamma' \\ [11\bar{1}]\alpha // [10\bar{1}]\gamma' \\ [\bar{2}1\bar{1}]\alpha // [\bar{1}2\bar{1}]\gamma' \end{aligned}$$

The recorded departure from this exact K–S orientation relationship [22] is shown in the Fig. 7.

Morphology of lamellar structure

The TEM image (Fig. 3), taken by tilting the pearlite at the edge-on orientation, allows us to estimate the interlamellar spacing to be about 150 nm. It should be noted that although the specimen was simply cooled in the furnace from austenite region and no quenching has been performed, the nitrogen pearlite exhibits a rather fine structure. The formation of the nitrogen pearlite (Fig. 8) follows the classical “branching” mechanism established by Hillert [23].

Many observations have shown that no apparent grain boundary is present between the proeutectoid and the pearlitic ferrites (Fig. 9a). This fact has been confirmed by electron diffraction. The Kikuchi diffraction patterns (Fig. 9b) recorded by moving the electron beam across the “virtual interface” (dotted line in Fig. 9) are the same

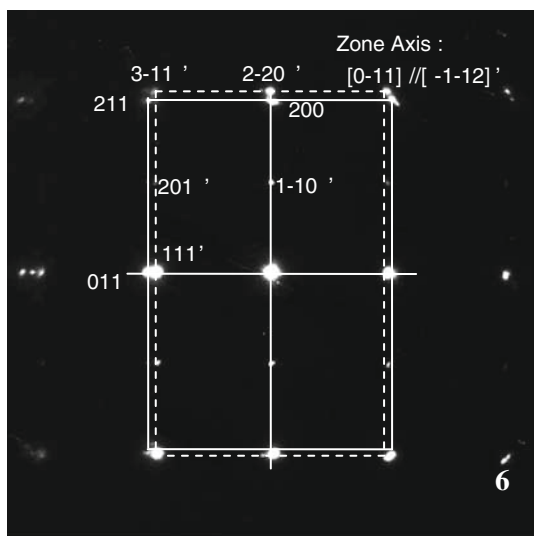


**Fig. 6** Diffraction pattern recorded along  $[0-11]\alpha$  (solid line) //  $[-1-12]\gamma'$  (dotted line) zone axis pointing out the N–W orientation relationship between the ferrite and the  $\gamma'$ -Fe<sub>4</sub>N nitride

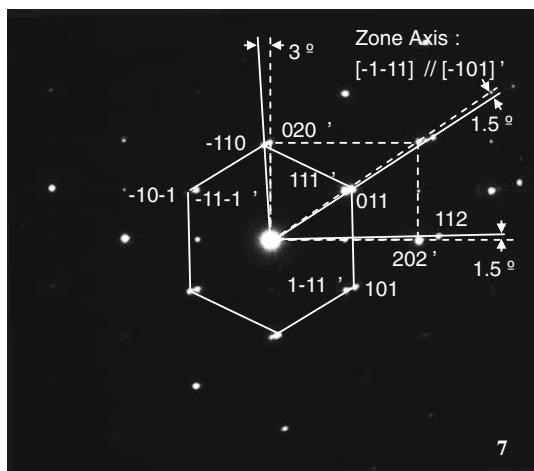


**Fig. 7** Diffraction pattern recorded along  $[-1-11]\alpha$  (solid line) //  $[-101]\gamma'$  (dotted line) zone axis pointing out a departure from the exact K–S orientation relationship:  $[011]\alpha$   $1.5^\circ$  from  $[111]\gamma'$

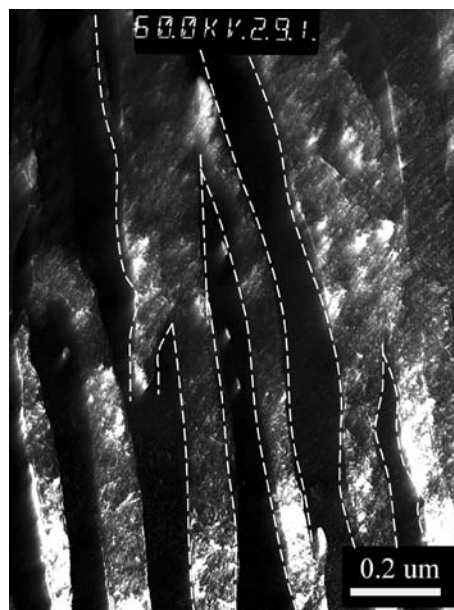


**Fig. 8** Dark-field TEM image showing the “branching” mechanism of the nitrogen–pearlite growth

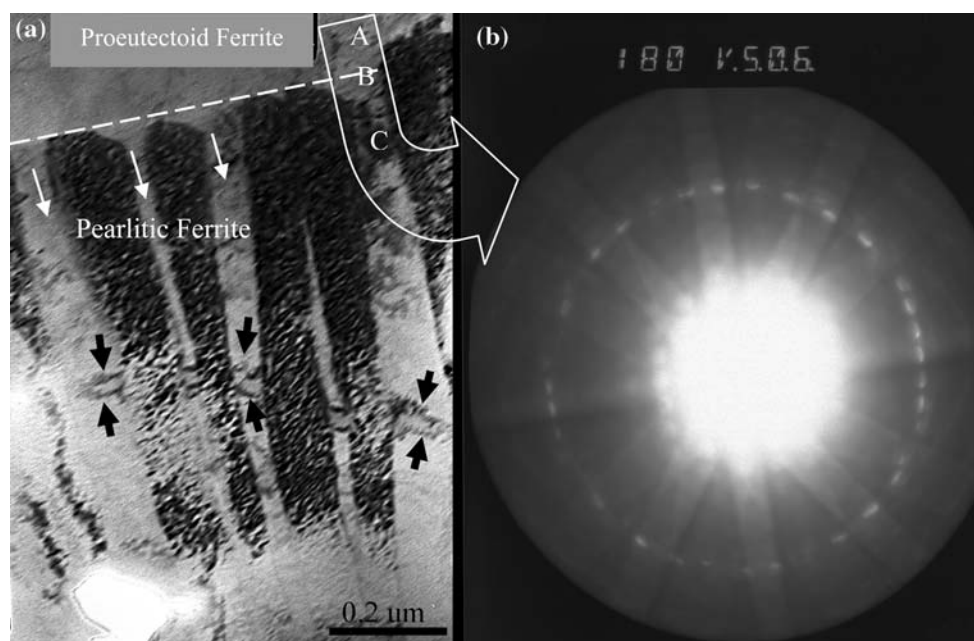


**Fig. 9** **a** Bright-field TEM images showing no grain boundary between proeutectoid (upper part) and pearlitic ferrites (lower part). **b** Kikuchi diffraction patterns at different points (A: proeutectoid

ferrite, B: virtual interface and C: pearlitic ferrite) are identical. A bend contour (black arrows) confirms that the pearlitic ferrite lamellas are oriented in the same direction

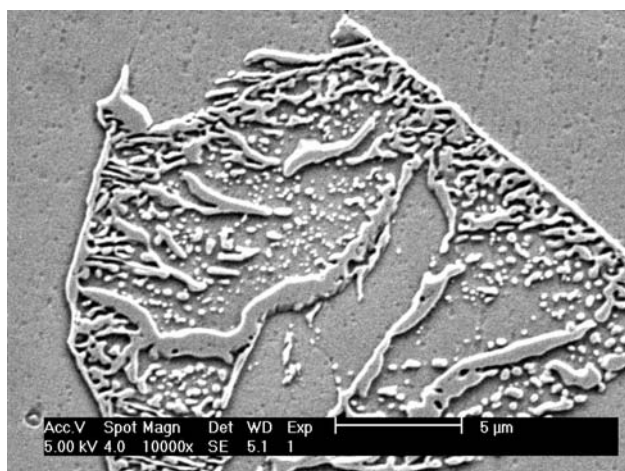


**Fig. 10** SEM micrograph of granular nitrogen pearlite

without any disorientation, indicating that the proeutectoid ferrite and the pearlitic ferrite are continuous. This result is consistent with many works on Fe–C hypoeutectoid steels [23–26], in which the proeutectoid ferrite is called the “active nucleus” for carbon pearlite formation in hypoeutectoid steels.

#### Morphology of granular and abnormal structure

The granular pearlitic structure has also been found. As is illustrated by SEM (Fig. 10) and TEM images (Fig. 11), the granular nitrides  $\gamma'$ -Fe<sub>4</sub>N, such as fine spherical

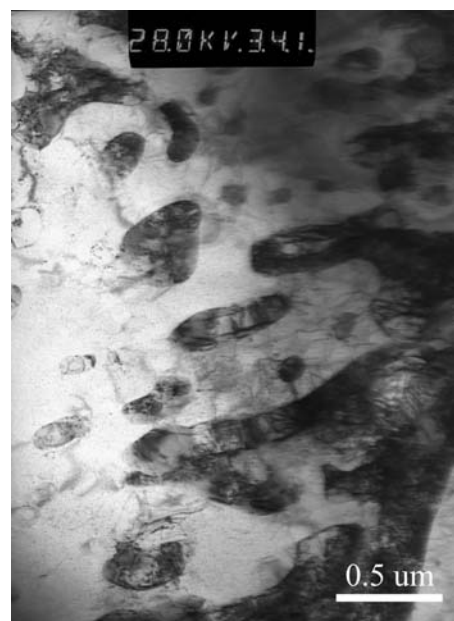


**Fig. 11** Bright-field TEM image of granular nitrogen pearlite: no specific orientation relationship between the ferrite and the globulized nitride  $\gamma'$ -Fe<sub>4</sub>N

precipitates forming in the ferrite matrix, lie in a thick layer of ferrite which intends to fill the grain of austenite. This granular structure, which is surrounded by an “abnormal structure” described by Hillert [23], shows strong tendency for coarsening.

**Table 1** Comparison of some important points on Fe–C and Fe–N phase diagrams

System	Eutectoid temperature (°C)	Solution solid elements composition C–N (wt%)		
		Ferrite (max)	Eutectoid point	Fe <sub>3</sub> C–Fe <sub>4</sub> N
Fe–C	727	0.02	0.77	6.67 in Fe <sub>3</sub> C
Fe–N	592	0.1	2.4	5.88 in Fe <sub>4</sub> N

No specific orientation relationship has been found between the ferrite and the granular nitride  $\gamma'$ -Fe<sub>4</sub>N although many electron diffractions have been made. This result is consistent with the work of Bell and Farnell [13]. The loss of orientation relationship may be related to the fact that the nitride  $\gamma'$ -Fe<sub>4</sub>N tends to minimize the strain energy during globulization and initially semi-coherent ferrite/nitride interfaces become non-coherent.

## Discussion

Several aspects in this study are necessary to be pointed out:

1. The crystal structure of  $\gamma'$ -Fe<sub>4</sub>N nitride has been confirmed to be  $P\frac{4}{m}\bar{3}\frac{2}{m}$ . The FOLZ reflections, belonging to all diffraction patterns, are very weak because they are only “produced” by nitrogen atoms. In fact the intensity of these FOLZ reflections is proportional to  $|F^{\text{FOLZ}}|^2 = f_N^2$ , compared to the ZOLZ reflection intensity, which is proportional to  $|F^{\text{ZOLZ}}|^2 = (4f_{\text{Fe}} \pm f_N)^2$ . In order to make these reflections visible, tilting the specimen is recommended.
2. The exact N–W and the near K–S orientation relationships between the ferrite and the  $\gamma'$ -Fe<sub>4</sub>N have been found in this study. The fact that the exact K–S relationship is not observed is not surprising because it is known that energetically the K–S orientation relationship is not a stable one [22]. Bell and Farnell [13] have found that the orientation relationship between the ferrite and the  $\gamma'$ -Fe<sub>4</sub>N is “within 11° of the Bain orientation relationship”. This result does not seem to be sufficiently accurate since the Bain orientation relationship can be produced from N–W one by a 9.74° rotation around [100]<sub>z</sub>, which is “within 11°”. So their results could be more precisely described by other specific orientation relationships.
3. It is interesting to compare the Fe–N pearlite with the Fe–C pearlite. Table 1 shows the important points on the phase diagram of the two systems.

In terms of mechanical properties, it is necessary to take into account three aspects:

- The nitrogen pearlite contains three times more hard phase ( $\gamma'$ -Fe<sub>4</sub>N is a well used hard phase in case treatment) than the carbon pearlite,
- The nitrogen ferrite containing 0.1 wt% of nitrogen, compared to carbon–nitrogen having much smaller carbon solubility (0.02 wt%), is supposed to have more solid solution reinforcement effect. These two aspects make the nitrogen pearlite probably harder than the carbon pearlite.
- The interlamellar spacing is a characteristic in the measurement of pearlite mechanical properties. In our study, although the specimen is simply cooled from austenite in the furnace and neither quenching nor further heat treatments have been done, the nitrogen pearlite exhibits a rather fine structure with the interlamellar spacing around 150 nm. This small interlamellar spacing, maybe related to the high diffusivity of nitrogen in  $\gamma'$ -Fe<sub>4</sub>N, suggests a good plasticity potential of the nitrogen pearlite. Therefore further attention should be paid on this issue.

Furthermore, the eutectoid temperature of the Fe–N system is 135 °C lower than that of the Fe–C system. This point makes it interesting to discuss some heat treatment ideas. For example, the pearlitic transformation could be realized at lower temperature as well as the further spheroidization treatment (if needed), therefore the energy consumption would be supposed to be lower.

**Acknowledgements** This work is financially supported by ArcelorMittal SA. One of the authors (A. R.) is grateful to Dr A. Handaj for helpful discussions.

## References

1. Kunze J (1990) Nitrogen and carbon in iron and steel thermodynamics. Akademie-Verlag, Berlin
2. Kunze J (1986) Steel Res 57:361
3. Agren J (1979) Metall Trans A 10A:1847
4. Hillert M, Jarl M (1975) Metall Trans A 6A:553
5. Pickering FB (1980) Tisco 27:105
6. Bell T, Owen WS (1967) J Iron Steel Inst 428
7. Gavriljuk VG, Berns H (1999) High nitrogen steels. Springer, Berlin
8. Jack DH, Jack KH (1973) Mater Sci Eng 11:1
9. Braune H (1905) Rev Mét 2:49
10. Fry A (1923) Kruppsche Monatshefte 4:138
11. Bose BN, Hawkes MF (1950) Trans AIME 188:307

12. Williams J et al (1968) In: Proceedings of international symposium by the Institute of Metals, University of Manchester, July 3 to 5, 1968, Monograph & Report Series No. 33, pp 49–53
13. Bell T, Farnell BC (1971) In: Proceedings of the international symposium on metallurgical chemistry—applications in ferrous metallurgy, Sheffield
14. Lehrer E (1930) *Z Elektrochem* 36:383
15. Xiong XC, Redjaïmia A, Goune M (2008) *J Mater Sci* (submitted)
16. Morniroli JP, Steeds JW (1992) *Ultramicroscopy* 45:219
17. Redjaïmia A, Morniroli JP (1994) *Ultramicroscopy* 53:305
18. Steeds JW, Vincent R (1983) *J Microsc Spectrosc Electron* 8:617
19. Nishiyama Z (1934) *Sci Rep Tohoku Univ* 23:638
20. Wasserman G (1933) *Arch Eisenhüttenwesen* 16:647
21. Kurdjumov G, Sachs G (1939) *Z Physik* 64:325
22. Cahn JW, Kalonji G (1982) In: Aaronson HI, Sekereka RF, Laughlin DE, Waymann CM (eds) Proceedings of the conference on solid-solid phase transitions, Metall Soc AIME, Warrendale
23. Hillert M (1962) Decomposition of austenite by diffusional processes. Interscience Publishers, New York
24. Modin S (1951) *Jernkont Ann* 135:169
25. Modin S (1958) *Jernkont Ann* 142:37
26. Thompson SW, Howell PR (1988) *Scripta Metallurgica* 22:1775